Monthly Notices
of the
ROYAL ASTRONOMICAL SOCIETY

The SAURON project -- IX. A kinematic classification for early-type galaxies.

Journal:	*Monthly Notices of the Royal Astronomical Society*
Manuscript ID:	MN-06-1171-MJ
Manuscript Type:	Main Journal
Date Submitted by the Author:	04-Aug-2006
Complete List of Authors:	Emsellem, Eric; Centre de Recherche Astrophysique de Lyon
Keywords:	galaxies: elliptical and lenticular, cD < Galaxies, galaxies: evolution < Galaxies, galaxies: formation < Galaxies, galaxies: structure < Galaxies, galaxies: kinematics and dynamics < Galaxies

Mon. Not. R. Astron. Soc. **000**, 000–000 (0000) Printed 4 August 2006 (MN LATEX style file v2.2)

The SAURON project – IX. A kinematic classification for early-type galaxies.

Eric Emsellem,[1] Michele Cappellari,[2] Davor Krajnović,[3] Glenn van de Ven,[2,4] R. Bacon,[1] M. Bureau,[3] Roger L. Davies,[3] P. T. de Zeeuw,[2] Jesús Falcón-Barroso,[2,5] Harald Kuntschner,[6] Richard McDermid,[2] Reynier F. Peletier,[7] Marc Sarzi,[3]

[1]*Université de Lyon 1, CRAL, Observatoire de Lyon, 9 av. Charles André, F-69230 Saint-Genis Laval; CNRS, UMR 5574 ; ENS de Lyon, France*
[2]*Sterrewacht Leiden, Niels Bohrweg 2, 2333 CA Leiden, The Netherlands*
[3]*Sub-Department of Astrophysics, University of Oxford, Denys Wilkinson Building, Keble Road, Oxford OX1 3RH, United Kingdom*
[4]*Department of Astrophysical Sciences, Peyton Hall, Princeton, NJ 08544, USA*
[5]*European Space and Technology Centre (ESTEC), Keplerlaan 1, Postbus 299, 2200 AG Noordwijk, The Netherlands*
[6]*Space Telescope European Coordinating Facility, European Southern Observatory, Karl-Schwarzschild-Str 2, 85748 Garching, Germany*
[7]*Kapteyn Astronomical Institute, Postbus 800, 9700 AV Groningen, The Netherlands*

4 August 2006

ABSTRACT

Two-dimensional stellar kinematics of 48 representative E and S0 galaxies obtained with the SAURON integral-field spectrograph reveal a wealth of structures. Early-type galaxies appear in two broad flavours, depending on whether they exhibit clear large-scale rotation or not. Using this unique dataset, we define a robust parameter $\lambda_R \equiv \langle R \cdot |V| \rangle \,/\, \langle R \cdot \sqrt{V^2+\sigma^2} \rangle$ as a proxy to quantify the observed angular momentum per unit mass. We use it as a basis for a new kinematic classification: early-type galaxies are separated into slow and fast rotators according to the measured value of λ_R. Slow and fast rotators are shown to be physically distinct classes of galaxies, a robust result which cannot simply be the consequence of a biased viewing angle. Three galaxies within the slow rotator class stand out, having the lowest λ_R values and being consistent with zero rotation (non-rotators): these are the three most massive ellipticals of our sample, have radio sources, are found near or at the centre of cluster potentials, and are known to have shallow inner surface brightness profiles and large Sersic shape indices. Fast rotators tend to be relatively low luminosity galaxies with $M_B > -20.5$. Slow rotators tend to be brighter and more massive galaxies, but are still spread over a wide range of absolute magnitude. As expected, the three non-rotators are the most massive and among the brightest galaxies in our sample. Remarkably, all other slow rotators (besides the atypical case of NGC 4550) contain a large kpc-scale kinematically decoupled core (KDC). All fast rotators which are not obviously barred show well aligned photometric and kinemetric axes, in contrast with most slow rotators which exhibit significant misalignments and do not show any hint of bars. These results are supported by the addition of 18 extra early-type galaxies observed with SAURON. We suggest that gas is a key ingredient in the formation and evolution of fast rotators, and that non-rotators are the extreme end point reached deep in gravitation potential wells where dissipationless mergers had a major role in the evolution. Detailed numerical simulations in a cosmological context are required to understand how to form large-scale KDCs within slow rotators, and more generally to explain the distinction between fast and slow rotators.

Key words: galaxies: elliptical and lenticular, cD – galaxies: evolution – galaxies: formation – galaxies: kinematics and dynamics – galaxies: structure

1 INTRODUCTION

The origin of the classification fork for galaxies can be found in an early paper by Jeans (1929), with the S0s as a class being introduced by Hubble (1936) to account for the important population of flattened objects in nearby clusters (Spitzer & Baade 1951). In a recent debate on galaxy classification, Sandage (2004) mentioned that the simplest definition of an S0 galaxy remains "a disc galaxy more flattened than an E6 elliptical but with no trace of spiral arms or recent star formation". Elliptical (E) and lenticular (S0) galaxies are usually gathered into the so-called early-type category, and are

recognised to share a number of global properties (de Vaucouleurs et al. 1991) such as their relatively low dust and interstellar gas content and their overall red colours. The Hubble sequence is however seen as a continuous one between ellipticals and spirals, with the S0s occupying the transition region with typical bulge to disc ratios of ~ 0.6. S0s are thus considered disc-dominated galaxies, while Es are spheroid-dominated.

Such contrived galaxy types may be misleading, most evidently because "the sequence E0-E6 is one of apparent flattening" (Kormendy & Bender 1996, hereafter KB96). A modern classification scheme should go beyond a purely descriptive tool, and should therefore encompass part of our knowledge of the physical properties of these objects[1]. This was advocated by KB96 who wished to update the Hubble sequence by sorting ellipticals in terms of the importance of rotation for their stellar dynamical state. They used the disciness or boxiness of the isophotes to quantify anisotropy and to define refined types: E(d) galaxies (for discy ellipticals) making the link between S0s and E(b) galaxies (for boxy ellipticals). The disciness (or boxiness) was then provided by a measure of the now classical normalised a_4/a term (see Bender et al. 1988, for details): positive and negative a_4 terms correspond to discy and boxy deviations from ellipses, respectively.

This extension of the Hubble types has the merit of upgrading our view of Es and S0s via some easily accessible observable parameter, and it follows the philosophy that a mature classification scheme should include some physics into the sorting criteria. It does, however, use a photometric indicator as an attempt to quantify the dynamical state of the galaxy, which may be unreliable. More importantly, it conserves the dichotomy between S0s and Es, relying on the old (and ambiguous) definition of an S0.

We have recently conducted a survey of 72 early-type (E, S0, Sa) galaxies using the integral-field spectrograph SAURON mounted on the William Herschel Telescope in La Palma (Bacon et al. 2001, hereafter Paper I; de Zeeuw et al. 2002, hereafter Paper II). This allowed us to map the stellar and gas kinematics as well as a number of stellar absorption line indices up to about one effective radius R_e for most of the galaxies in the sample. The two-dimensional stellar kinematics for the 48 E and S0 galaxies (Emsellem et al. 2004, hereafter Paper III) show a wide variety of features such as kinematically decoupled or counter-rotating cores, central discs and velocity twists. More importantly, there seem to be two broad classes of observed stellar velocity fields, with galaxies in one class exhibiting a clear large-scale rotation pattern and those in the other showing no significant rotation (Fig. 1). The existence of these two classes must be linked to the formation and evolution of early-type galaxies, and is in any case a key to understand their dynamical state (see also Cappellari et al. 2006b, hereafter Paper IV).

Using the unique dataset obtained in the course of the SAURON project, we here revisit the early-type galaxy classification issues mentioned above, using the available full two-dimensional kinematic information. A companion paper (Cappellari et al. 2006a, hereafter Paper X) examines in more detail the orbital anisotropy of elliptical and lenticular galaxies using the same data set. After a brief presentation of the dataset and methods (Sect. 2), we define a new parameter as a proxy to robustly quantify the angular momentum of galaxies (Sect. 3). In Section 4, we examine how this parameter relates both to the more standard measurement of V/σ and to the original de Vaucouleurs morphological classification of Es and S0s (de Vaucouleurs et al. 1991). We also discuss our new kinematic classification in the context of the more recent proposed revision of the Hubble sequence by KB96. We further conduct a detailed analysis of the photometric and kinematic properties of early-type galaxies in view of this new classification (Sect. 5). We then briefly discuss the implications of our results on the potential scenarios for the formation and evolution of these galaxies (Sect. 6), and conclude in Section 7.

[1] For the written transcript of a debate on this issue, see Sandage (2004) and the panel discussion in the same Proceedings.

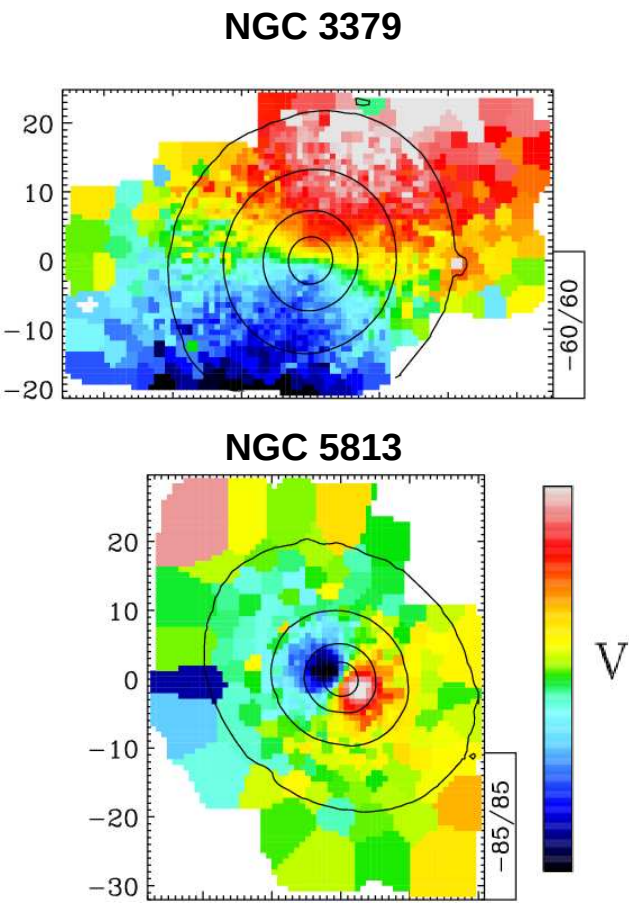

Figure 1. SAURON stellar velocity fields of NGC 3379 and NGC 5813, with overimposed isophotes (from Paper III; axes are in arcseconds). NGC 3379 exhibits a clear large-scale rotation pattern, in contrast to NGC 5813 which shows significant rotation in the central few arcseconds only.

2 DATA AND METHODS

2.1 The SAURON sample of E and S0s

The SAURON sample has been designed as a representative sample of 72 nearby ($cz < 3000$km s^{-1}) early-type galaxies in the plane of ellipticity ϵ versus absolute magnitude in the B band M_B. We restricted the sample to 24 objects for each of the E, S0 and Sa classes, with 12 'cluster' and 12 'field' targets in each group. In the present paper, we focus on the E+S0 sample which therefore contains 48 galaxies. More details about the full SAURON sample can be found in Paper II.

2.2 Photometry

Ground-based photometric MDM data (Falcón-Barroso et al. in preparation) was obtained for all galaxies of the SAURON sample. We also made use of additional HST/WPFC2 data which are available for 42 galaxies out of the 48 E/S0. Radial profiles for the ellipticity ϵ and a_4 parameters were obtained from these datasets using the GALPHOT package (Franx et al. 1989). We derived mean values by taking the flux weighted average of the corresponding profiles. More specifically, the mean $\overline{F}$ of a quantity $F(R)$, where R is the semi major-axis radius, is defined as

$$\overline{F} = \frac{\int_0^{R_{max}} q(R) R \cdot I(R) \cdot F(R) \mathrm{d}R}{\int_0^{R_{max}} q(R) R \cdot I(R) \mathrm{d}R} \quad (1)$$

where $q(R) = 1 - \epsilon(R)$ and $I(R)$ are respectively the best-fit ellipse axis ratio and surface brightness profile. Using the sampled radial profile, we approximate this with

$$\overline{F} \sim \frac{\sum_{i=1,n} q(R_i)(R\mathrm{max}_i{}^2 - R\mathrm{min}_i{}^2) I(R_i) F(R_i)}{\sum_{i=1,n} q(R_i)(R\mathrm{max}_i{}^2 - R\mathrm{min}_i{}^2) I(R_i)} \quad (2)$$

where $R\mathrm{min}_i$ and $R\mathrm{max}_i$ correspond to the inner and outer radii of the i^{th} annulus. The mean $(\overline{\epsilon})_e$ and $(\overline{a_4})_e$ within 1 R_e parameters are provided in Table 1. For both $(\overline{\epsilon})_e$ and $(\overline{a_4})_e$, the overall agreement between our values and published ones (Bender et al. 1994) is excellent (see Paper X for a comparison). In the following Sections, we denote $\overline{\epsilon}$ as the mean ellipticity within 1 R_e or restricted to the equivalent effective aperture of the SAURON field of view, whichever is smaller. This will be used in Sect. 3, where we examine kinematic quantities derived from SAURON data as a function of the flux weighted average ellipticity.

Results from fitting Sersic and Sersic-core laws (Trujillo et al. 2004; Ferrarese et al. 2006) to the obtained radial luminosity profiles will be presented in detail in a subsequent paper of this series (Falcón-Barroso et al., in preparation). In the present paper, we will only mention trends (Sect. 4.3), considering the Sersic index n (where $n = 1$ corresponds to an exponential luminosity profile, and $n = 4$ to a de Vaucouleurs $R^{1/4}$ law), as well as the classification of the central photometric profiles with either shallow or steep inner cusps, labelled respectively as "cores" and "power-laws" (Faber et al. 1997; Rest et al. 2001; Ravindranath et al. 2001; Lauer et al. 2005).

2.3 The SAURON data

SAURON is an integral-field spectrograph built at Lyon Observatory and mounted since February 1999 at the Cassegrain focus of the William Herschel Telescope. It is based on the TIGER concept (Bacon et al. 1995), using a microlens array to sample the field of view. Details of the instrument can be found in Paper I and II. All 48 E and S0 galaxies were observed with the low resolution mode of SAURON which covers a field of view of about $33'' \times 41''$ with $0\farcs94 \times 0\farcs94$ per square lens. Mosaicing was used to reach up to a radius of 1 R_e, which was managed for 25 galaxies out of the 48. Only for the two galaxies with the largest R_e (NGC 4486 and NGC 5846), we reach a radius of $\sim R_e/3$ only.

All data reduction was performed using the dedicated XSauron software wrapped in a scripted pipeline (Paper II). For each target, individual datacubes were merged and analysed as described in Paper III, ensuring a minimum signal-to-noise ratio of 60 per pixel using the binning scheme developed by Cappellari & Copin (2003). The SAURON stellar kinematics were derived using a penalised pixel fitting routine (Cappellari & Emsellem 2004), which provides parametric estimates of the line-of-sight velocity distribution (hereafter LOSVD) for each spaxel. In Paper III, we have presented the corresponding maps, which include the mean velocity V, the velocity dispersion σ and the Gauss-Hermite moments h_3 and h_4, for the 48 E and S0 SAURON galaxies.

As mentioned in Paper III, these quantities were measured fitting all V, σ, h_3 and h_4 simultaneously: this ensures an optimal representation of the corresponding LOSVD. In the present paper, we focus on the first two true velocity moments, μ_1 and μ_2, which are sometimes estimated by use of the Gauss-Hermite expansion of the LOSVD (van der Marel & Franx 1993). As emphasised in Paper IV, the second order moment is very sensitive to the details of the high velocity wings, which can rarely be accurately measured. We therefore decided to rely on a simpler but more robust single gaussian fit (excluding higher order moments), and used the gaussian mean V and standard deviation σ to approximate the first and second velocity moments.

2.4 Kinemetry

We employ a quantitative approach to analyse the SAURON stellar kinematic maps. Krajnović et al. (2006) recently advocated the use of a method generalising the isophotal-shape tools used for the analysis of photometry (Lauer 1985; Jedrzejewski 1987; Bender & Moellenhoff 1987). Maps of even moments, including the surface brightness, are treated similarly to the standard technique for photometry, expanding around ellipses of constant level. For maps of the odd moments, such as the mean velocity and the Gauss-Hermite parameter h_3, the zeroth order assumption is that the profile along an ellipse is a cosine law. The ellipse which minimizes the corresponding residuals is first derived, and the residuals are then expanded as a Fourier series. A more detailed account of the application of this technique can be found in Krajnović et al. (2006).

Applying kinemetry on a velocity map provides radial profiles for the kinematic position angle PA_{kin}, axis ratio q_{kin}, and Fourier kinemetry terms. Following Krajnović et al. (2006), we made use of the first and fifth terms k_1 and k_5 to characterize the stellar velocity maps, in addition to PA_{kin} and q_{kin}. The dominant term k_1 represents the velocity amplitude, and k_5 is the first term which does not define the best fitting ellipse. We define a kinematic component to have constant or slowly varying PA_{kin} and q_{kin} radial profiles (taking into account the derived error bars). A significant or abrupt change in at least one of these two parameters, or a double-hump structure in the velocity amplitude k_1, thus suggests the presence of two separate radial domains where different kinematic components dominate. More quantitatively, to identify two separate components, we require here either $\Delta q_k > 0.1$, or $\Delta \mathrm{PA}_{kin} > 10^\circ$, or a double-hump in k_1 with a local minimum in between. The transition between the two radial ranges is generally emphasised by a peak in the k_5 value, which thus serves as an additional signature for such a change (Krajnović et al. 2006). Velocity maps which exhibit the presence of at least two velocity structures are tagged as *Multiple Component* (MC), as opposed to a *Single Component* (SC).

We use a number of terms to represent some basic properties of the individual kinematic components using quantitative criteria, following the definitions provided in Krajnović et al. (2006, see also Krajnović et al. in preparation) :

- *Low-level velocity* (LV): defined when the maximum velocity amplitude k_1 is lower than 15 km s^{-1}. Note that when the velocity amplitude is constant over the field, PA_{kin} and q_{kin} are ill-defined.

- *Kinematic misalignment* (KM): defined when the absolute difference between the photometric PA_{phot} and PA_{kin} is larger than 10°.
- *Kinematic twist* (KT): defined by a smooth variation of the kinematic position angle PA_{kin} with an amplitude of at least 10° within the extent of the kinematic component.

We can now group galaxies depending on the *relative* characteristics of their individual kinematic components. A *kinematically decoupled component* (KDC) is defined as an MC having either an abrupt change in PA_{kin}, with a difference larger than 20° between two adjacent components, or with the outer kinematic component being LV (which prevents that component to have a robust PA_{kin} measurement). This definition roughly corresponds to the more standard appellation of KDC used in the past (Bender 1988), although the two-dimensional coverage provided by integral-field spectrographs allows a much more sensitive detection procedure. When the central kinematical component is LV, we label the galaxy as a central low-level velocity (CLV) system. These kinemetric groups will be discussed in Sect. 5.

3 QUANTIFYING THE ANGULAR MOMENTUM

The velocity fields presented in Paper III revealed a wealth of structures such as decoupled cores, velocity twists, misalignments, cylindrical or disc-like rotation (see also Section 5). It is however difficult to disentangle the relative contributions of a true variation in the internal dynamical state and the effect of projection. One way to further constrain the internal dynamics for a specific galaxy is to build a detailed model using all available observables. This was successfully achieved in Paper IV on a subsample of 24 galaxies, for which accurate distances and high spatial resolution photometry are available, and where no obvious signature of non-axisymmetry is observed. From these models, a considerable amount of detail on the orbital structure was derived (see also Paper X). We here design a simple parameter which quantifies the (apparent) *global* dynamical state of a galaxy, which is applicable to all galaxies in our representative sample of Es and S0s.

3.1 From $V_{\rm max}/\sigma_0$ to V/σ

The relation of V/σ versus mean ellipticity ϵ (hereafter the anisotropy diagram) was often used in the past to confront the apparent flattening with the observed amount of rotation (Illingworth 1977; Binney 1978; Davies et al. 1983). In the now classical treatment of the anisotropy diagram, the maximum observed rotational velocity $V_{\rm max}$ and the central dispersion σ_0 are generally used as surrogates for the mass-weighted mean of the square rotation speed and the random velocity. This was mostly constrained by the fact that stellar kinematics were available along at most a few axes via long-slit spectroscopy.

Binney (2005) has recently revisited this diagram to design a more robust diagnostic of the velocity anisotropy in galaxies using the two-dimensional kinematic information. Starting from the tensor Virial theorem, Binney reformulated the ratio of ordered versus random motions in terms of integrated quantities observable with modern integral-field spectrographs such as SAURON, namely $\langle V^2 \rangle$ and $\langle \sigma^2 \rangle$, where V and σ denote respectively the observed stellar velocity and velocity dispersion, and the brackets correspond to a sky averaging weighted by the surface brightness.

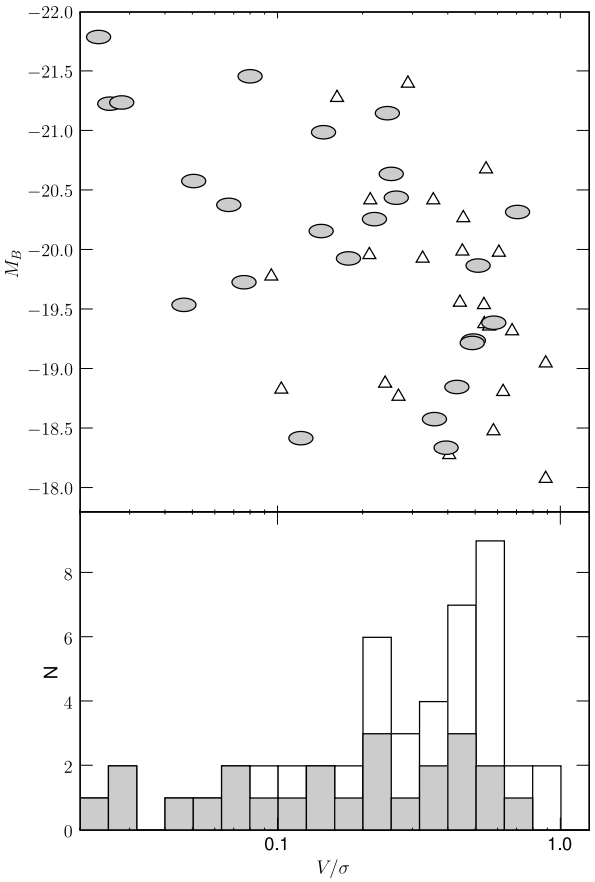

Figure 2. Top panel: total apparent magnitude M_B versus V/σ for the 24 E (grey ellipses) and 24 S0 (empty triangles) SAURON galaxies. The bottom panel shows the histograms of V/σ on a logarithmic scale for both the S0's (white) and E's (grey).

The SAURON data provide us with a unique opportunity to derive for the first time a robust measurement of V/σ for a sample of local early-type galaxies. We have therefore derived $\langle V^2 \rangle$ and $\langle \sigma^2 \rangle$ by spatially averaging the measured stellar velocity and velocity dispersion (squared) up to $\sim 1R_e$, weighted by the flux in each bin (see Paper X for details). The resulting V/σ values for the 48 SAURON E and S0 galaxies are given in Table 1 and shown in Fig. 2 as a function of their total absolute magnitude M_B, where symbols correspond to the Hubble type.

We observe a clear tendency for S0s to have higher V/σ than Es, as expected, and all galaxies with $V/\sigma < 0.09$ are classified as ellipticals. The three galaxies with the lowest V/σ values are also among the brightest ellipticals in our sample, with $M_B < -21.2$ mag. As emphasised in Paper X, which discusses the anisotropy diagram in the light of state-of-the art dynamical models, galaxies with relatively high V/σ (> 0.2) display a large range of ellipticities. This contrasts with galaxies with relatively low V/σ (< 0.2) which all have ellipticities $\overline{\epsilon} < 0.3$ except NGC 4550. NGC 4550 is in fact a nearly edge-on galaxy with two co-spatial counter-rotating stellar discs, each contributing for about 50% of the total luminosity, and should therefore be regarded as an atypical case where a high ellipticity is accompanied by a relatively low mean stellar velocity in the equatorial plane (see Paper X for a detailed discussion).

The value of V/σ, however, fails to provide us with a way to

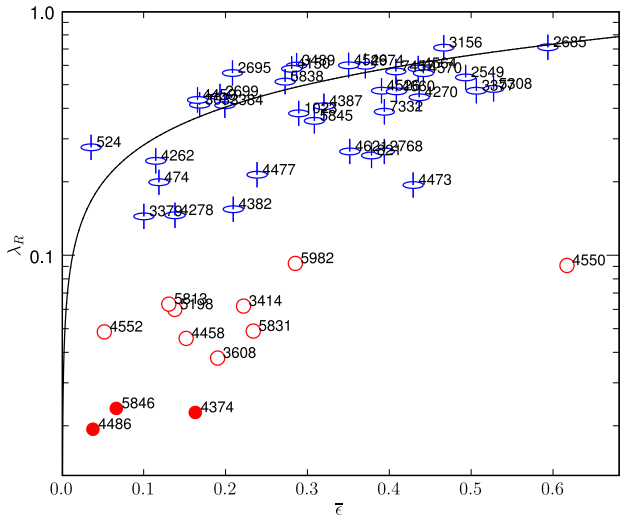

Figure 3. λ_R versus the mean ellipticity $\overline{\epsilon}$ for the 48 E and S0 galaxies of the SAURON sample. Slow rotators (which have $\lambda_R \leqslant 0.1$) are red circles, and fast rotators ($\lambda_R > 0.1$) are represented by special blue symbols (horizontal ellipse plus a vertical line). The filled circles are slow rotators for which $\lambda_R < 0.025$ (consistent with zero, see Appendix B). The black solid line corresponds to the curve $\mathcal{F}\left((V/\sigma)_{\rm iso}\right)$ versus $\overline{\epsilon}$ where $(V/\sigma)_{\rm iso}$ is the theoretical prediction for isotropic axisymmetric systems (with $\delta = \alpha = 0$, see Binney 2005), and $\mathcal{F}(x) = x/\sqrt{1+x^2}$ (see text).

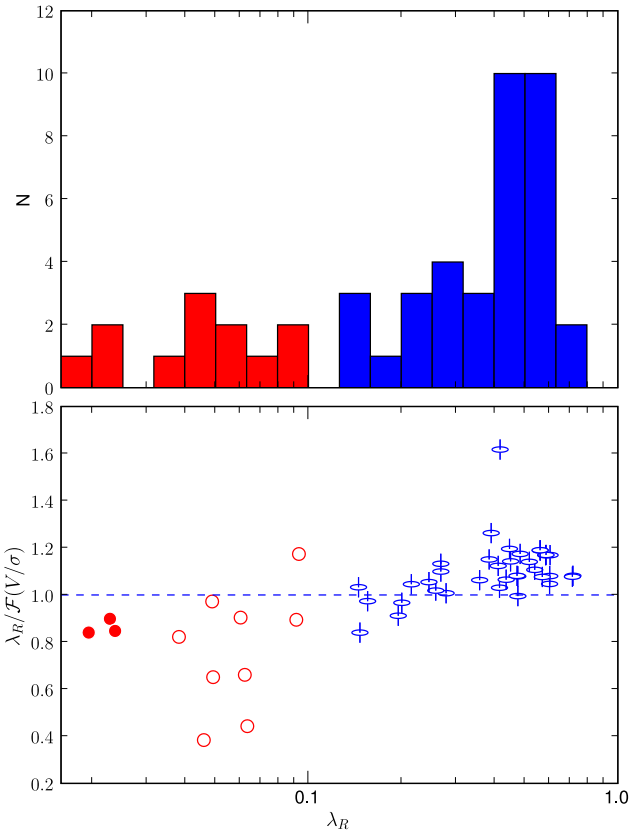

Figure 4. Top panel: histogram of λ_R values for the 48 E and S0 galaxies of the SAURON sample. Colour coding for slow rotators ($\lambda_R \leqslant 0.1$) and fast rotators ($\lambda_R > 0.1$) is the same as in Fig. 3. Bottom panel: ratio between λ_R and $\mathcal{F}(V/\sigma)$ as a function of λ_R, where $\mathcal{F}(x) = x/\sqrt{1+x^2}$. Symbols are as in Fig. 3. Note the large spread of slow rotators around $\lambda_R \sim 0.05$.

differentiate mean stellar velocity structures as different as those of NGC 3379 and NGC 5813 (see Figs. 1 and 2). These two galaxies have both $V/\sigma \sim 0.14$, and $\overline{\epsilon} \sim 0.1$, but their stellar velocity fields are qualitatively and quantitatively very different: NGC 3379 displays a regular and large-scale rotation pattern with a maximum amplitude of about 60 km s^{-1}, whereas NGC 5813 exhibits clear central KDC with a peak velocity amplitude of $\sim$ 85 km s^{-1} and a mean stellar velocity consistent with zero outside a radius of $\sim 12''$. The derivation of V/σ includes a luminosity weighting that emphasizes the presence of the KDC in NGC 5813. Although the maximum mean velocity measured in the SAURON field of view is only 40% higher in NGC 5813, these two galaxies end up with a similar V/σ.

3.2 From V/σ to λ_R : a new kinematic parameter

We therefore need to design a new practical way to quantify the global velocity structure of galaxies using the two-dimensional spatial information provided by integral-field units. The ideal tool would be a physical parameter which captures the spatial information included in the kinematic maps. Since we wish to assess the level of rotation in galaxies, this parameter should follow the nature of the classic V/σ: ordered versus random motion. A measure of the averaged angular momentum $\mathbf{L} = \mathbf{R} \wedge \mathbf{V}$, could play the role of V, and should be able to discriminate between large-scale rotation (NGC 3379) and little or no rotation (NGC 5813). Such a quantity, however, depends on the determination of the angular momentum vector direction, which is not an easily measured quantity. We therefore use a more robust and measurable quantity, $\langle R \cdot |V| \rangle$, where R is the observed distance to the galactic centre, as a surrogate for $\mathbf{L}$. A normalised parameter which makes use of the projected first two velocity moments (V and $V^2 + \sigma^2$) is then defined:

$$\lambda_R = \frac{\langle R \cdot |V| \rangle}{\langle R \cdot \sqrt{V^2 + \sigma^2} \rangle} \qquad (3)$$

The use of higher order moments of either V or the spatial weighting R would make this parameter more strongly dependent on the aperture and presence of noise in the data. Values of λ_R for the 48 E/S0 galaxies are provided in Table 1.

Figure 3 shows λ_R versus the mean ellipticity $\overline{\epsilon}$ for the 48 SAURON E and S0s, measured using an aperture of 1 R_e (or including the full SAURON field of view for galaxies with large R_e, see Sect. 3.3). Galaxies with $\lambda_R > 0.1$ all have velocity maps with significant large-scale rotation, and have ellipticities ranging up to about 0.6. We name these "fast rotators" hereafter (and colour them in blue). Apart from the atypical case of NGC 4550, galaxies with $\lambda_R < 0.1$ show little or spatially confined rotation and all have ellipticities $\overline{\epsilon} < 0.3$. These will be named "slow rotators" hereafter (and coloured in red). NGC 3379 and NGC 5813, which have similar V/σ, have as expected significantly different values of λ_R, and are then respectively fast and slow rotators.

Fast and slow rotators seem to be distinct classes, a result illustrated in Fig. 4. There are 36 fast rotators and 12 slow rotators (75% and 25% of the total sample), their median λ_R values being ~ 0.44 and 0.05 respectively. Within the class of slow rotators, three galax-

Table 1. Characteristics of the E and S0 galaxies in the representative SAURON sample. All galaxies with $\lambda_R > 0.1$ are classified as fast rotators.

Galaxy (1)	Type (2)	T (3)	M_B (4)	R_e (5)	$\overline{\epsilon}$ (6)	$(\overline{\epsilon})_e$ (7)	$(\overline{a_4/a})_e$ (8)	V/σ (9)	λ_R (10)	Group (11)	Rotator (12)
NGC474	$S0^0$(s)	-2.2	-20.42	29	0.12	0.13	-0.14	0.21	0.20	MC	F
NGC524	$S0^+$(rs)	-1.5	-21.40	51	0.04	0.04	-0.16	0.29	0.28	SC	F
NGC821	E6?	-4.2	-20.44	39	0.38	0.35	1.43	0.26	0.26	SC	F
NGC1023	$SB0^-$(rs)	-2.6	-20.42	48	0.29	0.36	0.54	0.35	0.38	SC	F
NGC2549	$S0^0$(r) sp	-2.0	-19.36	20	0.49	0.49	2.86	0.56	0.54	MC	F
NGC2685	(R)$SB0^+$pec	-0.7	-19.05	20	0.59	0.59	2.93	0.88	0.72	SC	F
NGC2695	$SAB0^0$(s)	-2.4	-19.38	21	0.21	0.21	0.36	0.54	0.56	MC	F
NGC2699	E:	-5.0	-18.85	14	0.19	0.19	1.04	0.43	0.45	MC	F
NGC2768	E6:	-3.1	-21.15	71	0.39	0.46	0.12	0.24	0.27	SC	F
NGC2974	E4	-3.6	-20.32	24	0.37	0.37	0.64	0.70	0.60	MC	F
NGC3032	$SAB0^0$(r)	-1.7	-18.77	17	0.17	0.17	0.44	0.27	0.42	CLV	F
NGC3156	S0:	-2.4	-18.08	25	0.47	0.47	-0.04	0.88	0.71	SC	F
NGC3377	E5-6	-4.0	-19.24	38	0.51	0.50	0.94	0.49	0.47	SC	F
NGC3379	E1	-4.0	-20.16	42	0.10	0.11	0.16	0.14	0.15	MC	F
NGC3384	$SB0^-$(s):	-2.6	-19.56	27	0.20	0.20	1.13	0.44	0.41	MC	F
NGC3414	S0 pec	-2.5	-19.78	33	0.22	0.23	1.80	0.09	0.06	KDC	S
NGC3489	$SAB0^+$(rs)	-2.1	-19.32	19	0.29	0.29	-0.61	0.67	0.60	MC	F
NGC3608	E2	-4.3	-19.54	41	0.19	0.20	-0.21	0.05	0.04	KDC	S
NGC4150	$S0^0$(r)?	-2.4	-18.48	15	0.28	0.28	-0.32	0.58	0.58	CLV	F
NGC4262	$SB0^-$(s)	-2.6	-18.88	10	0.11	0.11	1.28	0.24	0.25	MC	F
NGC4270	S0	-1.1	-18.28	18	0.44	0.44	-0.64	0.40	0.45	SC	F
NGC4278	E1-2	-4.6	-19.93	32	0.14	0.13	-0.15	0.18	0.15	MC	F
NGC4374	E1	-3.5	-21.23	71	0.16	0.13	-0.40	0.03	0.02	SC	S
NGC4382	$S0^+$(s)pec	-1.8	-21.28	67	0.21	0.22	0.59	0.16	0.16	CLV	F
NGC4387	E	-3.4	-18.34	17	0.32	0.32	-0.76	0.39	0.41	SC	F
NGC4458	E0-1	-3.8	-18.42	27	0.15	0.14	0.41	0.12	0.05	KDC	S
NGC4459	$S0^+$(r)	-2.0	-19.99	38	0.17	0.17	0.22	0.45	0.44	MC	F
NGC4473	E5	-4.2	-20.26	27	0.43	0.43	1.03	0.22	0.20	MC	F
NGC4477	SB0(s):?	-1.8	-19.96	47	0.24	0.23	2.04	0.21	0.22	MC	F
NGC4486	E0-1^+pec	-4.0	-21.79	105	0.04	0.07	-0.07	0.02	0.02	SC	S
NGC4526	$SAB0^0$(s):	-1.6	-20.68	40	0.39	0.41	-1.92	0.54	0.48	MC	F
NGC4546	$SB0^-$(s):	-2.6	-19.98	22	0.35	0.36	0.69	0.60	0.60	MC	F
NGC4550	$SB0^0$:sp	-2.3	-18.83	14	0.62	0.62	2.36	0.10	0.09	MC	F
NGC4552	E0-1	-3.4	-20.58	32	0.05	0.06	0.00	0.05	0.05	KDC	S
NGC4564	E	-4.1	-19.39	21	0.43	0.43	1.33	0.58	0.59	SC	F
NGC4570	S0 sp	-1.7	-19.54	14	0.44	0.44	1.90	0.53	0.56	MC	F
NGC4621	E5	-4.0	-20.64	46	0.35	0.35	1.66	0.25	0.27	KDC	F
NGC4660	E	-4.1	-19.22	11	0.41	0.41	0.66	0.49	0.47	MC	F
NGC5198	E1-2:	-3.4	-20.38	25	0.14	0.14	-0.17	0.07	0.06	KDC	S
NGC5308	$S0^-$ sp	-1.1	-20.27	10	0.53	0.53	4.74	0.45	0.48	MC	F
NGC5813	E1-2	-4.5	-20.99	52	0.13	0.17	-0.03	0.14	0.06	KDC	S
NGC5831	E3	-4.3	-19.73	35	0.23	0.20	0.46	0.08	0.05	KDC	S
NGC5838	$S0^-$	-3.0	-19.87	23	0.27	0.28	0.34	0.51	0.52	MC	F
NGC5845	E:	-4.1	-18.58	4	0.31	0.31	0.63	0.36	0.36	MC	F
NGC5846	E0-1	-4.2	-21.24	81	0.07	0.07	-0.38	0.03	0.02	SC	S
NGC5982	E3	-3.9	-21.46	27	0.28	0.28	-0.92	0.08	0.09	KDC	S
NGC7332	S0 pec sp	-1.7	-19.93	11	0.39	0.39	1.35	0.32	0.39	KDC	F
NGC7457	$S0^-$(rs)?	-2.2	-18.81	65	0.41	0.43	0.20	0.62	0.57	CLV	F

Notes: (1) Galaxy identifier. (2) Hubble type (NED). (3) Numerical morphological type (LEDA) (4) Absolute B magnitude (Paper II). (5) Effective radius, in arcsec. (6) Mean ellipticity within 1 R_e, or within the SAURON field of view when smaller (7) Mean ellipticity within 1 R_e (8) Mean isophote shape parameter a_4/a (in %) within 1 R_e (9) V/σ at 1 R_e (see text). (10) λ_R at 1 R_e (see text). (11) Kinemetry group (see Sect. 2.4). (12) Rotator class: F=fast, S=slow.

ies stand out, with λ_R significantly below 0.03. These are among the brightest galaxies of our sample, namely NGC 4486, NGC 4374 and NGC 5846. The measured λ_R is in fact an upper limit for these galaxies: their mean stellar velocity maps are consistent with zero rotation everywhere ("non-rotators"), and the measured values of $\lambda_R \sim 0.025$ are fully consistent with being entirely due to noise in the maps (see Appendix B).

As shown in Appendix B, we expect an overall correlation between V/σ and λ_R, with $\lambda_R \sim \mathcal{F}(V/\sigma)$ where $\mathcal{F}(x) = x/\sqrt{1+x^2}$. In fact, all galaxies in Fig. 3 lie close to or below the curve $\mathcal{F}\left((V/\sigma)_{\rm iso}\right)$ where $(V/\sigma)_{\rm iso}$ is the theoretical prediction for isotropic axisymmetric systems viewed edge-on (with $\delta = \alpha = 0$, see Binney 2005). The value of λ_R for a specific galaxy obviously depends on its internal dynamical status, is in some way related to the specific angular momentum (see Appendix A), and as a measure

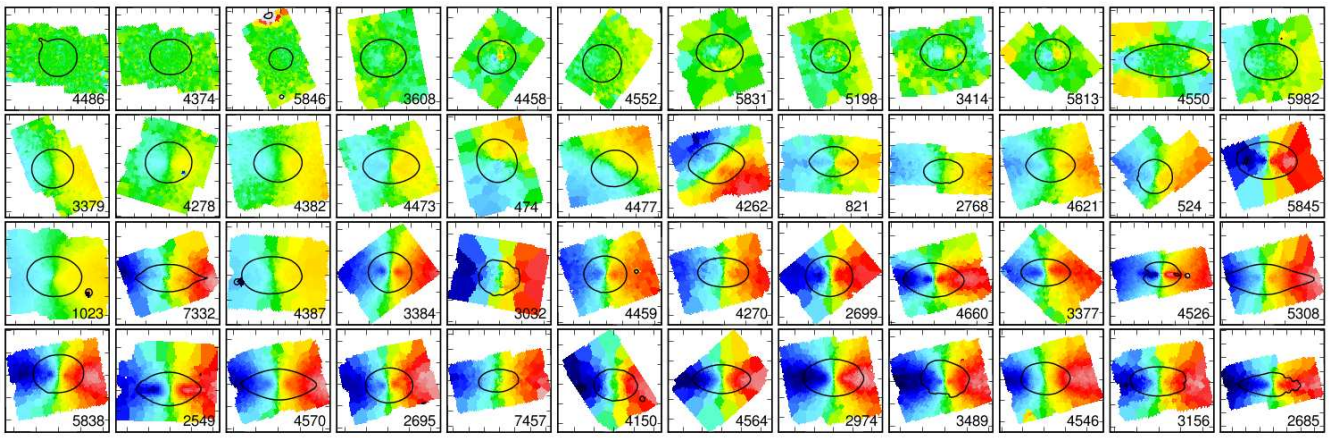

Figure 5. Stellar velocity fields as observed with SAURON for our 48 E and S0 galaxies, ordered by increasing value of λ_R (from left to right, top to bottom). Colour cuts were adapted for each galaxy according to $\sqrt{V^2+\sigma^2}$, as to mimic the normalisation included in λ_R. Slow rotators are galaxies on the first row, and fast rotators are galaxies in the bottom three rows. The maps have been oriented by aligning the global photometric axis horizontally. A representative isophote is overplotted in each thumbnail as a black solid line.

of projected quantities also strongly depends on the viewing angles. Assuming λ_R roughly follows the behaviour of $\mathcal{F}(V/\sigma)$ with the inclination angle i, a galaxy with a measured $\lambda_R = 0.05$, typical of observed slow rotators, would require to be at a nearly face-on inclination of $i \sim 20^\circ$ to reach an edge-on value of $\lambda_R \sim 0.15$, the smallest value for all observed fast rotators in our sample. It is therefore unlikely that the relative distribution of slow and fast rotators would significantly change even if all 48 galaxies were viewed edge-on.

The bottom panel of Fig. 4 illustrates the ratio between the measured values of λ_R and $\mathcal{F}(V/\sigma)$ for the 48 E/S0 SAURON galaxies. For galaxies with low λ_R, we observe a small bias due to the presence of noise in the kinematic maps (see Appendix B). The average spread around the best fit relation is only 10% for fast rotators, and more than 30% for slow rotators around $\lambda_R \sim 0.05$. Comparing $\mathcal{F}(V/\sigma)$ and λ_R values in Fig. 4, we clearly see that most fast rotators lie above, and most slow rotators lie below the 1:1 relation. Slow rotators therefore exhibit significantly lower stellar mean velocities at larger radii than fast rotators, where the radial weigthing included in the expression of λ_R becomes important. This clearly indicates distinct stellar kinematics between these two classes. This is further emphasised in Fig. 5, where we present the 48 SAURON stellar velocity fields ordered, from left to right, top to bottom, by increasing value of λ_R: fast rotators exhibit clear large-scale rotation patterns, in contrast to slow rotators. Slow rotators are therefore not simple scaled-down versions of fast rotators.

3.3 λ_R radial profiles

In the previous Section, we derived λ_R values using the SAURON two-dimensional kinematic maps available and a default equivalent aperture of 1 R_e. This aperture is covered by the SAURON datacubes for 17 galaxies out of the 48 in the SAURON E/S0 sample (see Paper IV), with two galaxies being mapped only to ~ 0.3 R_e (NGC 4486 and NGC 5846). As shown in Fig. 6, λ_R radial gradients vary significantly from galaxy to galaxy, so that we cannot confidently extrapolate λ_R to apertures much larger than constrained by the available data. The lack of a robust aperture correction for λ_R could cast doubts on our derived λ_R values and kinematic classification. However, Fig. 6 also shows that slow and fast rotators as defined in the previous Section exhibit qualitatively different λ_R profiles. Slow rotators have either decreasing or nearly flat (and small amplitude) λ_R profiles, and fast rotators preferentially exhibit increasing λ_R radial profiles. This is quantitatively illustrated in Fig. 7 which shows $\Delta\lambda_R$ the averaged radial gradient in $\lambda_R(R)$ with respect to λ_R: only five fast rotators (NGC 474, NGC 821, NGC 4278 and NGC 4473, NGC 5845) have a $\Delta\lambda_R$ value lower than the maximum gradient ($\Delta\lambda_R \sim 0.08$) measured in slow rotators. Furthermore, galaxies with the narrowest relative spatial coverage (with the largest R_e: NGC 4486, NGC 5846) are among the slowest rotators of our sample: these two galaxies are in fact known not to exhibit any significant rotation within 1 R_e (see Sembach & Tonry 1996), even though NGC 4486 (M 87) is in fact flattened at very large radii (see Kissler-Patig & Gebhardt 1998, and references therein). Considering this result, only very few galaxies near the $\lambda_R = 0.1$ threshold (e.g. NGC 5982, NGC 4550) could change their rotator class if we were to have a complete coverage up to 1 R_e.

4 HUBBLE TYPES AND PHOTOMETRY

In this Section, we examine in more detail potential links between the rotator classes defined in the previous Section, and some photometric properties of the galaxies in the SAURON sample.

4.1 Hubble Classification

There is a clear overlap of Es and S0s in the fast rotator class, with most of the corresponding galaxies having ellipticities higher than 0.2. This illustrates the fact that many Es have kinematic characteristics similar to S0s, and may therefore have embedded disc components (Bender 1988; Rix & White 1990). Ellipticals having such a disc contribution, quantified by a positive a_4/a, were classified as "discy" ellipticals or E(d) by KB96.

It seems difficult, however, to distinguish between a so-called E(d) and an S0 galaxy from the anisotropy diagram alone. KB96 argued that E(d)s are objects intermediate between S0s and boxy ellipticals or E(b)s (ellipticals with boxy isophotes, i.e. negative a_4/a). In principle, the Ed-S0-Sa sequence is one of decreasing

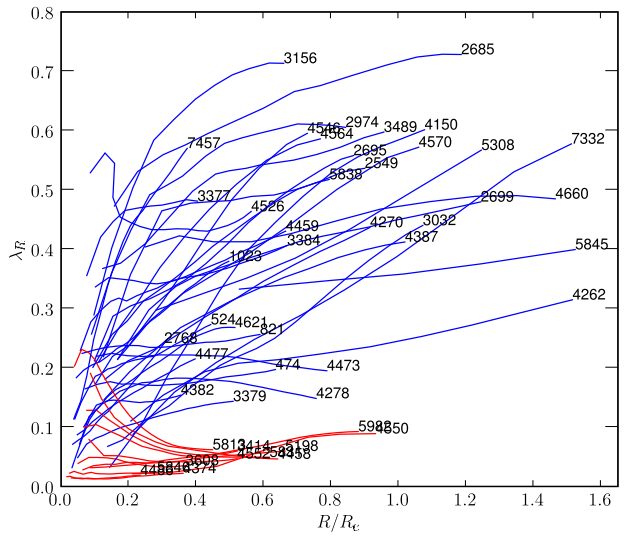

Figure 6. Radial λ_R profiles for the 48 E and S0 galaxies of the SAURON sample. Profiles of slow and fast rotators are coloured in red and blue, respectively.

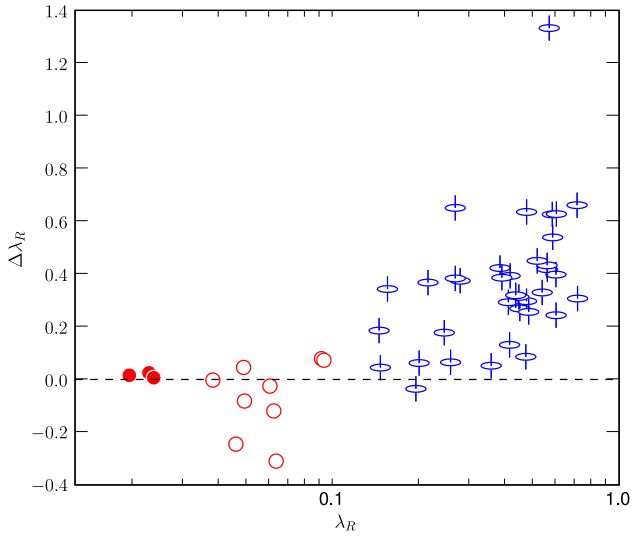

Figure 7. Average radial λ_R gradient within 1 R_e $\Delta\lambda_R$ for the 48 E and S0s of our SAURON sample, versus λ_R. Symbols are as in Fig. 3.

bulge-to-total light ratio (B/T), with S0s having $B/T \sim 0.6$ in the B band (Fritze v. Alvensleben 2004). B/T is, however, a fairly difficult quantity to measure in early-type galaxies, as it depends on the adopted ad-hoc model for the surface brightness distribution of the disc and bulge components. As emphasised by de Jong et al. (2004), the kinematic information is critical in assessing the rotational support of both components.

Consider two galaxies of our sample, NGC 3377 and NGC 2549, which both have similar V/σ and λ_R, the former being classified as a discy elliptical, the latter as a lenticular. Both have very similar total luminosity, $V-I$ colour (Tonry et al. 2001) and gas content (Sarzi et al. 2006, hereafter Paper V). Their SAURON stellar kinematic maps look also quite similar (Paper III), with large-scale disc-like rotation, a centrally peaked stellar velocity dispersion and a significant h_3 term, anti-correlated with the mean

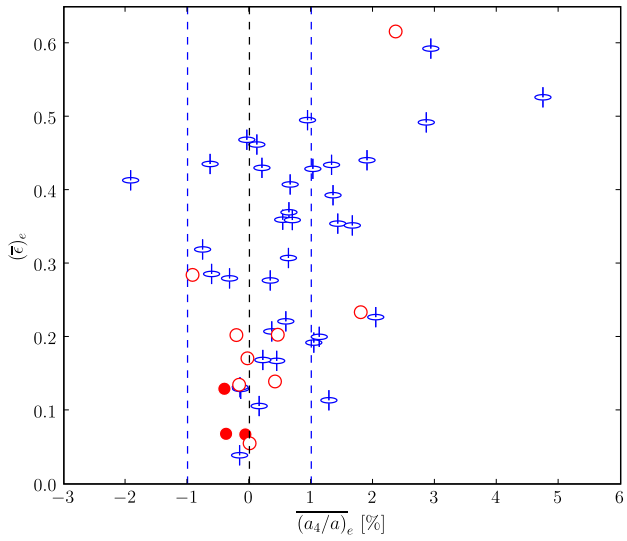

Figure 8. Mean ellipticity $(\overline{\epsilon})_e$ versus mean $\overline{(a_4/a)}_e$ (in %) within 1 R_e. Symbols for slow and fast rotators are as in Fig. 3.

velocity. Finally, there is some evidence that NGC 3377 contains a bar, with its velocity map exhibiting a stellar kinematical misalignment and a spiral-like ionised gas distribution (Paper V). This therefore strongly argues for NGC 3377 to be a misclassified barred S0 (an SAB0). Following the same lines of argument, we suggest that most and possibly all of the 14 Es which are fast rotators are misclassified S0s. This trend without doubt extends to all Es, a conclusion similar to one previously reached by a number of authors mostly on the basis of photometry alone (e.g. van den Bergh 1990; Michard 1994; Jorgensen & Franx 1994).

4.2 Isophote shapes

KB96 mention that a_4/a can be used as a reasonably reliable way to measure velocity anisotropy. They first observe, using $(V/\sigma)^\star$ (V/σ normalised to the value expected for an isotropic edge-on oblate system), that discy galaxies ($a_4 > 0$) seem consistent with near isotropy, whereas boxy galaxies ($a_4 < 0$) spread over a large range of $(V/\sigma)^\star$ values. However, as emphasised by Binney (2005) and in Paper X, $(V/\sigma)^\star$ is not a good indicator of anisotropy: the relation between $(V/\sigma)^\star$ and the anisotropy of a galaxy strongly depends on its flattening, as well as on its inclination (Burkert & Naab 2005). More flattened galaxies will thus tend to lie closer to the $(V/\sigma)^\star = 1$ curve, which explains in part why galaxies with discy and boxy isophotes seem to extend over different ranges of $(V/\sigma)^\star$, the former being then incorrectly interpreted as near-isotropic systems. This suggests we should avoid using $(V/\sigma)^\star$ at all, and leads us to examine more directly the orbital anisotropy of galaxies (see Binney 2005). This is achieved in Paper X, in which a trend between the anisotropy parameter in the meridional plane and the average intrinsic ellipticity is revealed (see their Fig. 7), more *flattened* galaxies tending to be more *anisotropic*. The latter study also convincingly shows that slow and fast rotators cannot be described by a single shape distribution. This contradicts the view that discy galaxies are nearly isotropic, and we should therefore reexamine the relation between the isophotal shape as measured by a_4 and the kinematic status of early-type galaxies.

KB96 presented a fairly significant correlation between the mean ellipticity $\overline{\epsilon}$ and $\overline{a_4/a}$ for their sample of early-type galaxies

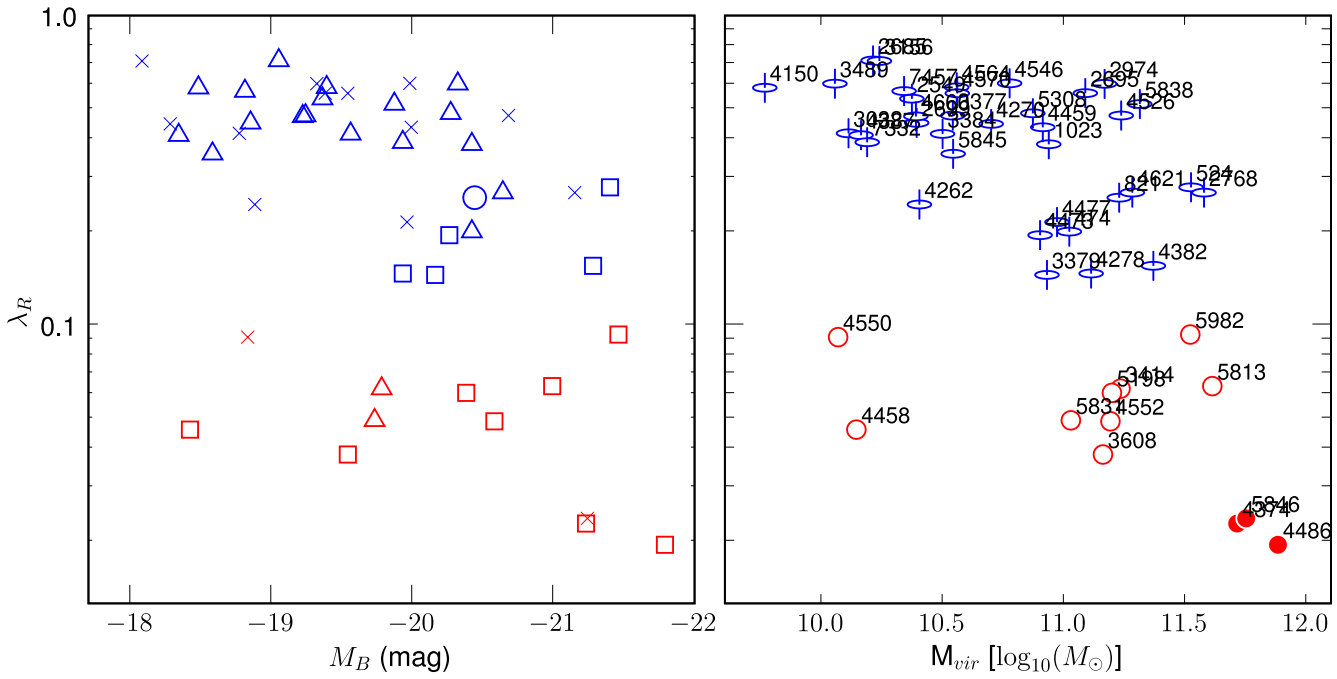

Figure 9. λ_R versus absolute magnitude M_B (left panel) and Virial mass M_{vir} (right panel) for the 48 E and S0 of the SAURON sample. In the left panel, symbols correspond to the cusp slope classification (Faber et al. 1997; Rest et al. 2001; Ravindranath et al. 2001; Lauer et al. 2005) with power-laws as triangles, cores as squares, NGC 821 which is an "intermediate" object as a circle, and crosses indicating galaxies for which there is no published classification. In the right panel, symbols for slow and fast rotators are as in Fig. 3.

(their Fig. 3). They mentioned that galaxies in a $\overline{\epsilon}$ versus $\overline{a_4/a}$ diagram exhibit a V-shaped distribution. The authors therefore pointed out that this remarkable correlation implies that early-type galaxies with nearly elliptical isophotes are also nearly round, and galaxies with the most extreme $\overline{a_4}$ values are also the most flattened (see also Hao et al. 2006). We confirm this result using our photometric data on the SAURON sample as shown in Fig. 8. As mentioned above, all slow rotators with the exception of NGC 4550 have ellipticities $\overline{\epsilon}$ lower than 0.3, and our expectation that these galaxies should have isophotes close to pure ellipses is verified: 9 out of 11 have $\left|\overline{(a_4/a)_e}\right| < 0.5\%$, the two exceptions being the boxy galaxy NGC 5982 which has $\lambda_R \sim 0.1$ (see Sect. 3.3), and NGC 3414, for which the relatively large positive a_4 value comes from the remarkable polar-ring structure (van Driel et al. 2000).

In fact, most fast rotators have a *maximum* absolute $|(a_4/a)|$ value within 1 R_e larger than 2%, whereas most slow rotators (with the exceptions again of NGC 3414 and NGC 4550) have *maximum* absolute $|(a_4/a)|$ values less than 2%. This means that most fast rotators in the SAURON sample of E and S0 galaxies exhibit significantly non-elliptical isophotes, but most slow rotators do not. However, we do not detect a clear correlation between the boxiness and the angular momentum per unit mass as quantified by λ_R in the galaxies of our sample, although there is a tendency for fast rotators to have positive $\overline{a_4}$ (discy isophotes). This seems partly in contradiction with the claim by KB96 that rotation is dynamically less important in boxy than in discy early-type galaxies. The latter result probably originated from the combination of two observed facts: firstly boxy galaxies are on average less flattened (extremely flattened galaxies are very discy), and secondly the use of $(V/\sigma)^\star$ as a proxy for the amount of organised rotation in the stellar component, which tends to underestimate the rotational support for less flattened galaxies. As emphasised in Paper X, there is in fact a trend that indicates that more flattened galaxies seem to be more strongly anisotropic.

4.3 Luminosity and mass

In the left panel of Fig. 9, we show the distribution of λ_R as a function of absolute magnitude M_B for the 48 SAURON E/S0 galaxies. As already emphasised above, the three non-rotators (NGC 4486, NGC 4374, NGC 5846) are among the brightest galaxies in our sample with $M_B < -21$ mag. Other slow rotators tend to be bright but are spread over a wide range of absolute magnitude going from the relatively faint NGC 4458, to brighter objects such as NGC 5813. The bright and faint end of slow rotators can be distinguished by the shapes of their isophotes: slow rotators with $M_B < -20$ mag all exhibit mildly boxy isophotes (negative a_4 with amplitude less than 1%) while the four discy slow rotators are all fainter than $M_B > -20$ mag, following the known correlation between the isophote shapes and the total luminosity of early-type galaxies (Bender et al. 1992). Most fast rotators are fainter than $M_B > -20.5$ mag, and all galaxies with $\lambda_R > 0.3$ have $M_B > -20.7$ mag.

Going from total luminosity to mass, we have estimated the latter by approximating it with the Virial mass M_{vir} derived from the best-fitting relation obtained in Paper IV, namely $M_{vir} \sim 5.0\, R_e \sigma_e^2/G$, where σ_e is the luminosity weighted second velocity moment within 1 R_e (see Paper IV for details). The calculation of M_{vir} from observables depends on the distance of the object, which we obtained from different sources for the galaxies in our sample (in order of priority, from Tonry et al. 2001; Tully 1988, and from the LEDA database assuming a Hubble flow with $H = 75$ km.s^{-1}.Mpc^{-1}). A trend of λ_R tending to be lower for more massive galaxies clearly emerges if we now use this esti-

mate of the Virial mass M_{vir} (right panel of Fig. 9), as expected from the one observed with absolute magnitude M_B (left panel of Fig. 9). The three non-rotators have the three highest values of M_{vir} in our sample. Except for NGC 4458 and NGC 4550, all slow rotators have $M_{vir} > 10^{11}$ $M_\odot$, whereas most fast rotators have $M_{vir} < 10^{11}$ $M_\odot$, lower masses being reached as the value of λ_R increases. There is a clear overlap in mass between fast rotators with intermediate values of λ_R (between 0.1 and 0.3) and slow rotators.

Irrespectively of the debated existence of a bimodality between cores and power-laws galaxies (Ravindranath et al. 2001; Lauer et al. 2005), it is then interesting to examine if there is a link between the specific angular momentum as measured by λ_R and the slope of the inner luminosity profile: 33 out of the 48 SAURON galaxies have published cusp classification (Faber et al. 1997; Rest et al. 2001; Ravindranath et al. 2001; Lauer et al. 2005). As illustrated in the left panel of Fig. 9, we find that most slow rotators are core galaxies, and most fast rotators are power-law galaxies. Galaxies with intermediate values of λ_R ([0.1–0.2]) are in fact mostly core galaxies, and NGC 821 which has an $\lambda_R \sim 0.25$ is specified as an "intermediate" object between a core and power-law (Lauer et al. 2005). These results are expected as there is a known trend between the central luminosity gradient and the total luminosity of early-type galaxies, bright members tending to be core galaxies, and lower luminosity ones to have power-law profiles (Faber et al. 1997). This is however not a one-to-one correspondence since a few power-law galaxies are observed as slow rotators (NGC 3414 and NGC 5813), and at least one fast rotator (NGC 524) is classified as a core galaxy. All galaxies with $\lambda_R < 0.3$ are fainter than $M_B = -20.7$ (as mentioned above), and are power-laws, but below $\lambda_R = 0.3$ we find both faint and bright galaxies, as well as cores and power-laws. Another interesting result is found when examining the larger-scale luminosity profiles of galaxies in our sample via the representation by a Sersic law. Besides the atypical case of NGC 4550, all slow rotators have Sersic index $n > 4$: again, this is expected since galaxies with larger Sersic shape index tend to be brighter (Graham & Guzmán 2003). Finally, galaxies with the lowest Sersic n values are also among the fastest rotators. A more detailed account regarding these issues will be provided in Falcón-Barroso et al. (in preparation).

5 KINEMETRIC STRUCTURES

We now turn to the kinemetric profiles (see Sect. 2.4) of the 48 SAURON galaxies, which allow us to determine the number of observed kinematic components and their individual characteristics. We thus make use of the average photometric and kinematic position angles and axis ratio (PA_{phot} and PA_{kin}, q and q_{kin}), and the average and maximum of the velocity amplitude k_1.

5.1 Kinemetry groups

The kinemetric groups of the observed 48 SAURON velocity maps, defined in Sect. 2.4, are provided in Table 1. 34 out of 48 galaxies in this sample (70%) exhibit multiple components (MC), including 11 kinematically decoupled components (KDCs; 23%) and 4 objects with central low-level velocity (CLVs), namely NGC 3032, NGC 4150, NGC 4382, and NGC 7457. Two more galaxies with KDCs are in fact at the limit of being CLVs (NGC 4621 and NGC 7332) with a maximum velocity for their inner component

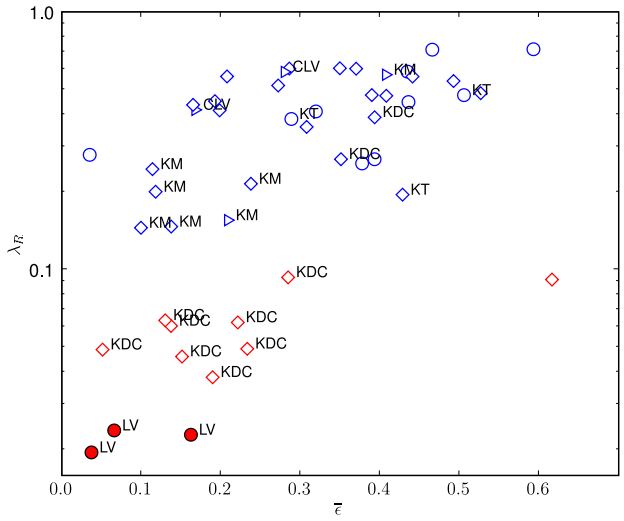

Figure 10. λ_R versus mean ellipticity $\overline{\epsilon}$, with indications of the velocity structures identified in Sect. 2.4. Galaxies with MCs are shown as diamonds, SCs as circles, and CLVs as right triangles. Colours for slow and fast rotators are as in Fig. 3.

around 20 km s^{-1} at the SAURON resolution. The latter two galaxies as well as the CLVs have in fact all been shown to harbour small counter-rotating stellar systems (Falcón-Barroso et al. 2004; Wernli et al. 2002; McDermid et al. 2006): it is the lower spatial resolution of the SAURON data which produces the low central velocity gradient. Among the KDCs, 5 galaxies (NGC 3414, NGC 3608, NGC 4458, NGC 5813, NGC 5831) have outer LV components. Kinematic misalignments are observed in 12 galaxies (25%), and 6 galaxies have individual kinematic components which have kinematical twists (KTs, 2 of them also having kinematical misalignements - KM). Considering the difficulty of detecting these structures at certain viewing angles or low spatial resolution, the number of such detected velocity structures is a lower limit.

In Fig. 10 we again show the $(\lambda_R, \overline{\epsilon})$ diagram (as in Fig. 3), now with the characteristic velocity structures detected via kinemetry. The first obvious fact is that the three non-rotator galaxies, which have the lowest λ_R values, are tagged as low-velocity (LV) systems. As mentioned above, these three galaxies form a distinct group within the slow rotator class, all three being bright giant round ellipticals with $M_B < -21$. Apart from these three and the atypical case of NGC 4550, all other slow rotators harbor KDCs, the central kinematic component having a typical size of 1 kpc or larger (see McDermid et al. 2006, hereafter Paper VIII). This contrasts with KDCs and CLVs in fast rotators (NGC 3032, NGC 4150, NGC 7332, NGC 7457), where the size of the central (counter-rotating) stellar component is only a few arcseconds in radius, corresponding to significantly less than 500 pc (Paper VIII).

The fast rotators with intermediate values of λ_R between 0.1 and 0.3 all show a kinematic misalignment or twist (KM, KT), or a KDC, except for NGC 821. For $\lambda_R > 0.3$, there are 4 fast rotators with a velocity twist or misalignment (KT, KM), or KDC, and all of them are barred (NGC 1023, NGC 3377, NGC 7332, NGC 7457). Most of the galaxies with multi-components but no specific velocity structures are among the fastest rotators. This result may be partly understood if these objects tend to be close to edge-on, which renders the detection of such velocity structures harder, but the detection of multiple discs easier.

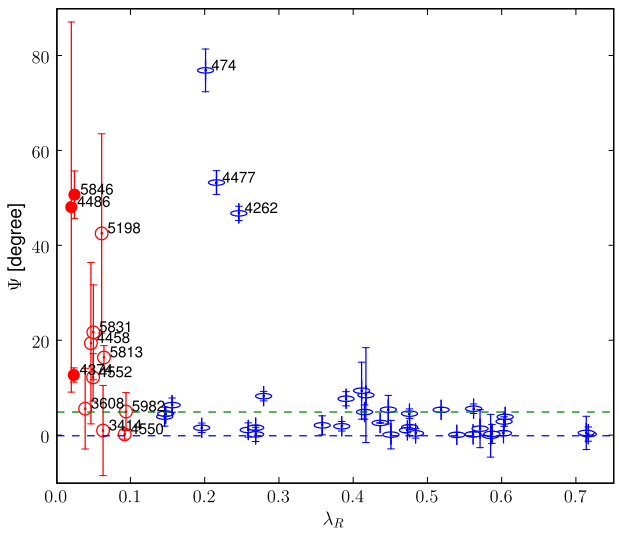

Figure 11. Kinematic misalignment Ψ between the global photometric major-axis and the kinematic axis within the SAURON field with respect to λ_R. Nearly all fast rotators have small Ψ values ($< 10°$). The 3 fast rotators which have $\Psi > 10°$ exhibit obvious bars. This contrast with slow rotators which show significantly non-zero Ψ values, but are not barred.

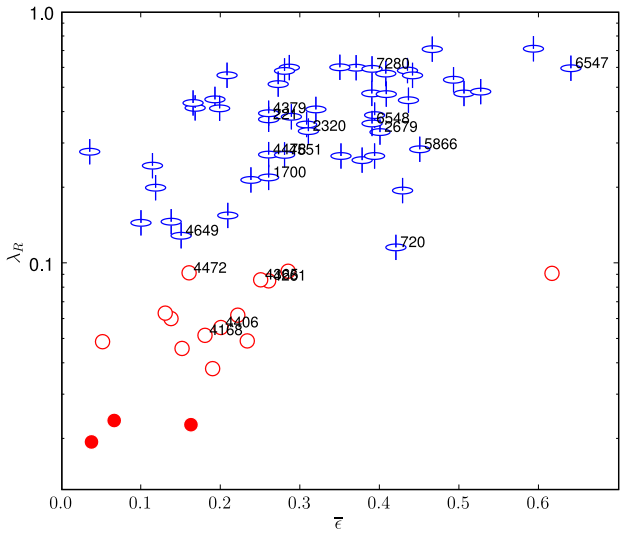

Figure 12. λ_R versus the ellipticity $\overline{\epsilon}$ including the additional 18 E and S0 galaxies observed with SAURON(labelled with NGC numbers). Symbols are the same as in Fig. 3.

5.2 Kinematic Misalignments

The fact that slow rotators exhibit distinct kinematics can also be demonstrated by considering the global alignment (or misalignment) between photometry and kinemetry. Fig. 11 illustrates this by showing the kinematic misalignment Ψ for all 48 E and S0 galaxies in the SAURON sample. Note that the photometric PA is derived using the large-scale MDM data, but the kinematic PA via a global measurement on the SAURON velocity maps as described in Krajnović et al. (2006). All fast rotators except three have misalignments Ψ below $10°$. The three exceptions are NGC 474, NGC 4262 and NGC 4477, which have obvious strong bars. In fact, the few galaxies which have $5° < \Psi < 10°$ are also almost certainly barred (NGC 3377, NGC 3384, NGC 4382, NGC 7332). In contrast, more than half of all slow rotators have $\Psi > 10°$, but none of these exhibit any hint of a bar. This difference in the misalignment values of slow and fast rotators cannot be entirely due to the effect of inclination, not only because of the argument mentioned in Sect. 4.2, but also because even the roundest fast rotators do not exhibit large misalignment values (see Sect. 5.1 in Paper X).

6 DISCUSSION

The fast rotators are mostly discy galaxies exhibiting multiple components in their stellar velocity fields. Contrarily to slow rotators, the main stellar kinematic axis in fast rotators is relatively well aligned with the photometric major-axis, except for the obvious strongly barred cases. This result together with the fact that λ_R profiles are qualitatively different for slow and fast rotators clearly show that slow rotators are not velocity scaled-down versions of fast rotators. The small number of galaxies in our sample, as well as our biased representation of the galaxy luminosity function, reminds us that a larger and complete sample is required to reveal the true λ_R distribution in early-type galaxies. The results mentioned above nevertheless remain when we include 18 additional early-type galaxies observed with SAURON (Fig. 12), the most remarkable fact being the confirmation that within these 18 extra targets, there are 5 slow rotators (NGC 4168, NGC 4406, NGC 4472, NGC 4261, NGC 4365), which *all* contain large (kpc) scale KDCs.

Interpreting the measured kinematic parameter λ_R as a proxy for the amount of angular momentum per unit mass in the central region of early-type galaxies (see Appendix A), we can then discuss the origin of this angular momentum. The standard scenario for the formation of galaxy structures includes hierarchical clustering of cold dark matter halos within which gas is cooling (Peebles 1969; Doroshkevich 1970; White 1984). The angular momentum of the dark matter halos is thought to originate in cosmological torques and major mergers (e.g. Vitvitska et al. 2002), this hypothesis providing a reasonable frame for the formation of disc galaxies. If major mergers produce a significant increase in the specific angular momentum of the dark matter halos at large radii (Vitvitska et al. 2002), minor mergers seem to just preserve or only slightly increase it with time (D'Onghia & Burkert 2004). But little is known on the expected distribution of the angular momentum of the *baryons* (van den Bosch et al. 2002; de Jong et al. 2004), and even less if we focus on the central regions of galaxies (within a few effective radii). In fact, discs formed in numerical simulations are generally an order of magnitude too small (but see Dutton et al. 2006, for a possible solution).

Numerical simulations, whether they include a dissipative component or not, have helped us to understand how mergers influence the rotational support of the baryonic component in galaxies (see e.g. Barnes 1998; Somerville & Primack 1999; Cole et al. 2000; Bournaud et al. 2005; Naab et al. 2006). Stellar discs are cold and fragile systems, thus easily destroyed during major mergers which often lead to elliptical-like remnants even in the presence of a moderate amount of gas (Naab et al. 2006). Intermediate to minor mergers preserve part of the disc better, but in most cases a merger leads to a redistribution of the angular momentum of the central stellar component outwards (Bournaud et al. 2004).

In this context, fast rotators have either preserved or regained their specific angular momentum in the central part. Since both very gas-rich major and minor mergers seem to produce fast (disc-

dominated) rotators (Robertson et al. 2006; Cox et al. 2006), this requires either the absence of a major dry merger, or reforming a disc-like system via gas accretion. At high redshift ($z > 2$), gas was abundant, and very gas-rich mergers should have therefore been common. Robertson et al. (2006) in fact claim that progenitors of early-type galaxies must be gas-rich (gas fraction $> 30\%$) to produce the fundamental plane (FP) tilt. Dry major mergers are therefore expected to occur preferentially at lower z, with fast rotators not having suffered from such events. In the picture of the hierarchical formation of structures, minor mergers are more common than major mergers and we can thus expect galaxies to have suffered from more than one of these events up to $z = 0$.

The resulting specific angular momentum of fast rotators, as quantified by λ_R, is therefore expected to result mostly from a competition between (i) gas-rich minor mergers or other inflow of external gas that causes a gradual increase of λ_R (in the inner parts), and (ii) dissipationless dry minor mergers triggering disc instability and heating, and resulting in the transformation of disc material into a spheroidal component, lowering λ_R (in the inner parts). The scenario described here follows the idea previously sketched by many authors (e.g. Kormendy & Bender 1996; Faber et al. 1997; Naab et al. 2006) that dissipation is important in the formation process of fast rotating early-type galaxies. The 'heating' of the disc via star formation leads to an increase in the vertical dispersion, more isotropic and rounder galaxies, and therefore moving the galaxies along the anisotropy–ellipticity trend (Paper X) towards the slow rotators. A sudden removal of the gas (e.g., due to AGN feedback or ram pressure stripping) might have 'quenched' this process, and quickly moved the galaxy from the 'blue cloud' to the 'red sequence' (Faber et al. 2005). Some galaxies may still have recently accreted some gas (e.g. via interaction with a companion, see Falcón-Barroso et al. 2004), and sometime show the presence of a younger stellar population (such as NGC 3032, NGC 3489, NGC 4150, see Kuntschner et al. 2006, and Paper VIII). In fact all SAURON E/S0 galaxies which have luminosity weighted ages of their stellar component lower than 6 Gyr are fast rotators (Fig. 13; see also Kuntschner et al. in preparation). Among the 16 galaxies in our sample with have the highest ionised gas content ($> 5\,10^{-7}$ of the total mass), only 2 are slow rotators, namely NGC 3414 with a relatively low M_{gas}/M_{vir} of $\sim 7\,10^{-7}$, and the atypical disc galaxy NGC 4550.

Following the same line of argument, slow rotators need to have expelled most of their angular momentum within one effective radius outwards. This would require a significant fraction of the mass to be accreted during mergers with relatively gas-poor content. As emphasised above, all slow rotators with $\lambda_R > 0.03$ (thus excluding the three non-rotators) have stellar kpc-size KDCs. According to numerical simulations, the formation of such structures still seem to require the presence of some gas during the merger process followed by subsequent star formation, either in equal-mass mergers (Naab et al. 2006) or in multiple intermediate or minor mergers (Bournaud, PhD Thesis, Paris). Fig. 13 reveals that most slow rotators have a relatively modest fraction of ionised gas and are in fact older than 8 Gyr. The only two exceptions are, again, NGC 4550 which is very probably the result of the rare encounter of two disc galaxies with nearly exactly opposite spins (see Paper X), and NGC 3414 which shows the "rudiments of a disc" (Sandage & Bedke 1994), and photometric structures reminiscent of polar-ring galaxies(van Driel et al. 2000) presumably formed via a tidal gas accretion event (Bournaud & Combes 2003). These results are consistent with the suggestion that slow rotators did not suffer from significant (in mass) recent dry mergers which tend to

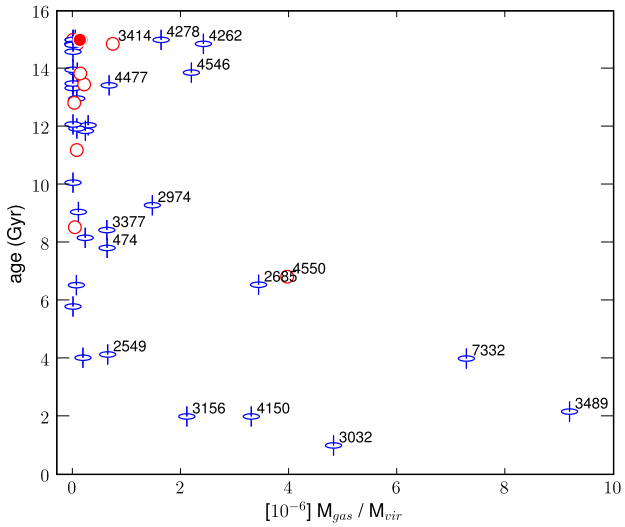

Figure 13. Average luminosity-weighted age of the stellar component versus the specific mass of ionised gas within the SAURON field of view M_{gas}/M_{vir} (ionised gas mass normalised by the Virial mass, see Sect. 4.3). Symbols for fast and slow rotators are as in Fig. 3. Numbers for the ionised gas specific mass are derived from values in Papers IV and V, and average luminosity-weighted ages are from Kuntschner et al. (in preparation).

destroy the large-scale KDCs. Minor mergers may still have recently occured, and as above result in a competition of (slightly) lowering and increasing λ_R.

Non-rotators such as NGC 4374, NGC 4486, and NGC 5846 are then the extreme end point of early-type galaxy evolution where dry mergers had a major role in the evolution, allowing λ_R to reach values consistent with zero in the central region. These galaxies are all found near or at the centre of cluster potentials (cDs and BCGs) and hence are expected to have experienced many mergers with galaxies which were themselves gas-depleted (due to ram-pressure stripping, efficient AGN feedback, or to earlier mergers), preferentially on radial orbits along the cosmological filaments (Boylan-Kolchin et al. 2006). As for the other slow-rotators, the initial mergers will have been gas-rich to place them on the FP, but later-on dry mergers are expected to be frequent as galaxies fall into the cluster potential well. The insignificant role of star formation in the late history of these galaxies is reflected in both their extremely low specific gas content and old luminosity weighted ages (Fig. 13). Overall, the trend we observe for early-type galaxies to have lower λ_R with increasing mass (Fig. 9) is consistent with the gradually more important role of (gas-poor) mergers when going from fast rotators, to slow rotators and to non-rotators.

7 CONCLUSIONS

Using two-dimensional stellar kinematics, we have argued that early-type galaxies can be divided into two broad dynamical classes, those that exhibit large-scale rotation and those that do not. We have devised a new parameter λ_R to quantify the specific angular momentum in the stellar component of galaxies. This parameter, as applied within one effective radius to the 48 E and S0 galaxies of our SAURON sample, allowed us to disentangle the two classes of fast and slow rotators with a threshold value of 0.1. We have shown in Sect. 3.3 that fast and slow rotators exhibit different stellar kinematics (see also Paper X). This also ensures that the measured λ_R

values are representative even though we do not fully cover the region within one effective radius for all sample galaxies. Our classification scheme is thus robust.

Beside the obvious difference in their angular momentum content, the main properties of the fast and slow rotators are as follows:

(i) 75% of the galaxies in our sample are fast rotators, 25% are slow rotators. Most of the slow rotators are classified as Es, while fast rotators include a mix of Es and S0s.

(ii) Within the slow rotators, we identify a subclass of three giant early-type galaxies for which the velocity field is consistent with nearly zero rotation (non-rotators). These three objects (NGC 4374≡M 84, NGC 4486≡M 87 and NGC 5846) are all massive nearly round galaxies in very dense environments, and have bright and compact radio cores. These are the so-called giant ellipticals (cDs or BCGs), which are known to have large Sersic shape index, and shallow inner surface brightness profiles (Faber et al. 1997).

(iii) Fast rotators have ellipticities up to $\overline{\epsilon} \sim 0.6$, in contrast to slow rotators which are relatively round systems with $\overline{\epsilon} < 0.3$.

(iv) Fast rotators tend to be relatively low-luminosity objects with $M_B > -20.7$. Slow rotators cover almost the full range of absolute magnitude of our sample, from faint discy galaxies such as NGC 4458 to bright slightly boxy galaxies such as NGC 5813, although they on average tend to be brighter than fast rotators. All slow rotators have Sersic index n larger than 4.

(v) More than 70% of the galaxies in our sample exhibit Multi-Component kinematic systems. Fast rotators have nearly aligned photometric and kinematic components, except for the obvious more face-on barred galaxies such as NGC 474, NGC 4262 and NGC 4477. This contrast with slow rotators which have significant kinematic misalignments.

(vi) All slow rotators, besides the three non-rotators, exhibit a kiloparcsec-scale stellar KDC (see Sect. 5.1 and PaperVIII).

These results are all confirmed when including 18 additional galaxies observed with SAURON. Although our sample of 48 early-type galaxies is not a good representation of the galaxy luminosity distribution in the nearby Universe, it is the first to provide such a constraint for numerical simulations of galaxy formation and evolution. It is clear that a significantly larger and unbiased sample is required to probe the true distribution of λ_R in early-type galaxies and the fraction of slow and fast rotators. Even so, our sample should serve as a reference point for detailed numerical simulations of galactic systems in a cosmological context.

ACKNOWLEDGMENTS

We thank Frank van den Bosch for useful discussions. The SAURON project is made possible through grants 614.13.003, 781.74.203, 614.000.301 and 614.031.015 from NWO and financial contributions from the Institut National des Sciences de l'Univers, the Université Claude Bernard Lyon I, the Universities of Durham, Leiden, and Oxford, the Programme National Galaxies, the British Council, PPARC grant 'Observational Astrophysics at Oxford 2002–2006' and support from Christ Church Oxford, and the Netherlands Research School for Astronomy NOVA. RLD is grateful for the award of a PPARC Senior Fellowship (PPA/Y/S/1999/00854) and postdoctoral support through PPARC grant PPA/G/S/2000/00729. The PPARC Visitors grant (PPA/V/S/2002/00553) to Oxford also supported this work. MC acknowledges support from a VENI grant 639.041.203 awarded by the Netherlands Organization for Scientific Research (NWO). JFB acknowledges support from the Euro3D Research Training Network, funded by the EC under contract HPRN-CT-2002-00305. This paper is based on observations obtained at the William Herschel Telescope, operated by the Isaac Newton Group in the Spanish Observatorio del Roque de los Muchachos of the Instituto de Astrofísica de Canarias. This project made use of the HyperLeda and NED databases. Part of this work is based on data obtained from the ESO/ST-ECF Science Archive Facility. Photometric data were obtained (in part) using the 1.3m McGraw-Hill Telescope of the MDM Observatory.

REFERENCES

Bacon R., Adam G., Baranne A., Courtes G., Dubet D., Dubois J. P., Emsellem E., Ferruit P., Georgelin Y., Monnet G., Pecontal E., Rousset A., Say F., 1995, A&AS , 113, 347

Bacon R., Copin Y., Monnet G., Miller B. W., Allington-Smith J. R., Bureau M., Carollo C. M., Davies R. L., Emsellem E., Kuntschner H., Peletier R. F., Verolme E. K., de Zeeuw P. T., 2001, MNRAS , 326, 23

Barnes J. E., 1998, in Kennicutt Jr. R. C., Schweizer F., Barnes J. E., Friedli D., Martinet L., Pfenniger D., eds, Saas-Fee Advanced Course 26: Galaxies: Interactions and Induced Star Formation Dynamics of Galaxy Interactions. pp 275–+

Bender R., 1988, A&A , 202, L5

Bender R., Burstein D., Faber S. M., 1992, ApJ , 399, 462

Bender R., Doebereiner S., Moellenhoff C., 1988, A&AS , 74, 385

Bender R., Moellenhoff C., 1987, A&A , 177, 71

Bender R., Saglia R. P., Gerhard O. E., 1994, MNRAS , 269, 785

Binney J., 1978, MNRAS , 183, 501

Binney J., 2005, MNRAS , 363, 937

Bournaud F., Combes F., 2003, A&A , 401, 817

Bournaud F., Combes F., Jog C. J., 2004, A&A , 418, L27

Bournaud F., Jog C. J., Combes F., 2005, A&A , 437, 69

Boylan-Kolchin M., Ma C.-P., Quataert E., 2006, MNRAS , 369, 1081

Burkert A., Naab T., 2005, MNRAS , 363, 597

Cappellari M., Bacon R., Bureau M., Damen C., Davies R. L., de Zeeuw P. T., Emsellem E., Falcón-Barroso J., Krajnović D., Kuntschner H., McDermid R. M., Peletier R. F., Sarzi M., van den Bosch R. C. E., van de Ven G., 2006a, MNRAS

Cappellari M., Bacon R., Bureau M., Damen M. C., Davies R. L., de Zeeuw P. T., Emsellem E., Falcón-Barroso J., Krajnović D., Kuntschner H., McDermid R. M., Peletier R. F., Sarzi M., van den Bosch R. C. E., van de Ven G., 2006b, MNRAS

Cappellari M., Copin Y., 2003, MNRAS , 342, 345

Cappellari M., Emsellem E., 2004, PASP , 116, 138

Cole S., Lacey C. G., Baugh C. M., Frenk C. S., 2000, MNRAS , 319, 168

Cox T. J., Dutta S. N., Di Matteo T., Hernquist L., Hopkins P. F., Robertson B., Springel V., 2006, ArXiv Astrophysics e-prints

Davies R. L., Efstathiou G., Fall S. M., Illingworth G., Schechter P. L., 1983, ApJ , 266, 41

de Jong R. S., Kassin S., Bell E. F., Courteau S., 2004, in Ryder S., Pisano D., Walker M., Freeman K., eds, IAU Symposium Properties of Dark Matter Halos in Disk Galaxies. pp 281–+

de Jong R. S., Simard L., Davies R. L., Saglia R. P., Burstein D., Colless M., McMahan R., Wegner G., 2004, MNRAS , 355, 1155

de Vaucouleurs G., de Vaucouleurs A., Corwin Jr. H. G., Buta R. J., Paturel G., Fouque P., 1991, Third Reference Catalogue of Bright Galaxies. Volume 1-3, XII, 2069 pp. 7 figs.. Springer-Verlag Berlin Heidelberg New York

de Zeeuw P. T., Bureau M., Emsellem E., Bacon R., Carollo C. M., Copin Y., Davies R. L., Kuntschner H., Miller B. W., Monnet G., Peletier R. F., Verolme E. K., 2002, MNRAS , 329, 513

D'Onghia E., Burkert A., 2004, ApJ , 612, L13

Doroshkevich A. G., 1970, Astrophysics, 6, 320

Dutton A. A., van den Bosch F. C., Dekel A., Courteau S., 2006, ArXiv Astrophysics e-prints

Emsellem E., Cappellari M., Peletier R. F., McDermid R. M., Bacon R., Bureau M., Copin Y., Davies R. L., Krajnović D., Kuntschner H., Miller B. W., de Zeeuw P. T., 2004, MNRAS , 352, 721

Faber S. M., Tremaine S., Ajhar E. A., Byun Y.-I., Dressler A., Gebhardt K., Grillmair C., Kormendy J., Lauer T. R., Richstone D., 1997, AJ , 114, 1771

Faber S. M., Willmer C. N. A., Wolf C., et al. 2005, ArXiv Astrophysics e-prints

Falcón-Barroso J., Peletier R. F., Emsellem E., Kuntschner H., Fathi K., Bureau M., Bacon R., Cappellari M., Copin Y., Davies R. L., de Zeeuw T., 2004, MNRAS , 350, 35

Ferrarese L., Côté P., Jordán A., Peng E. W., Blakeslee J. P., Piatek S., Mei S., Merritt D., Milosavljević M., Tonry J. L., West M. J., 2006, ApJS , 164, 334

Franx M., 1988, Structure and kinematics of elliptical galaxies. Leiden: Rijksuniversiteit, 1988

Franx M., Illingworth G., Heckman T., 1989, AJ , 98, 538

Fritze v. Alvensleben U., 2004, in Block D. L., Puerari I., Freeman K. C., Groess R., Block E. K., eds, Penetrating Bars Through Masks of Cosmic Dust On the Origin of SO Galaxies. pp 81–+

Graham A. W., Guzmán R., 2003, AJ , 125, 2936

Hao C. N., Mao S., Deng Z. G., Xia X. Y., Wu H., 2006, ArXiv Astrophysics e-prints

Hubble E. P., 1936, Yale University Press

Illingworth G., 1977, ApJ , 218, L43

Jaffe W., 1983, MNRAS , 202, 995

Jedrzejewski R. I., 1987, MNRAS , 226, 747

Jorgensen I., Franx M., 1994, ApJ , 433, 553

Kissler-Patig M., Gebhardt K., 1998, AJ , 116, 2237

Kormendy J., Bender R., 1996, ApJ , 464, L119+

Krajnović D., Cappellari M., de Zeeuw P. T., Copin Y., 2006, MNRAS , 366, 787

Kuntschner H., Emsellem E., Bacon R., Bureau M., Cappellari M., Davies R. L., de Zeeuw P. T., Falcón-Barroso J., Krajnović D., McDermid R. M., Peletier R. F., Sarzi M., 2006, MNRAS , 369, 497

Lauer T. R., 1985, MNRAS , 216, 429

Lauer T. R., Faber S. M., Gebhardt K., Richstone D., Tremaine S., Ajhar E. A., Aller M. C., Bender R., Dressler A., Filippenko A. V., Green R., Grillmair C. J., Ho L. C., Kormendy J., Magorrian J., Pinkney J., Siopis C., 2005, AJ , 129, 2138

McDermid R. M., Emsellem E., Shapiro K., Bacon R., Bureau M., Cappellari M., Davies R. L., de Zeeuw P. T., Falcón-Barroso J., Krajnović D., Kuntschner H., Peletier R. F., Sarzi M., 2006, MNRAS , p. submitted

Michard R., 1994, A&A , 288, 401

Naab T., Jesseit R., Burkert A., 2006, ArXiv Astrophysics e-prints

Naab T., Khochfar S., Burkert A., 2006, ApJ , 636, L81

Peebles P. J. E., 1969, ApJ , 155, 393

Ravindranath S., Ho L. C., Peng C. Y., Filippenko A. V., Sargent W. L. W., 2001, AJ , 122, 653

Rest A., van den Bosch F. C., Jaffe W., Tran H., Tsvetanov Z., Ford H. C., Davies J., Schafer J., 2001, AJ , 121, 2431

Rix H.-W., White S. D. M., 1990, ApJ , 362, 52

Robertson B., Bullock J. S., Cox T. J., Di Matteo T., Hernquist L., Springel V., Yoshida N., 2006, ApJ , 645, 986

Robertson B., Cox T. J., Hernquist L., Franx M., Hopkins P. F., Martini P., Springel V., 2006, ApJ , 641, 21

Sandage A., Bedke J., 1994, The Carnegie atlas of galaxies. Washington, DC: Carnegie Institution of Washington with The Flintridge Foundation, —c1994

Sarzi M., Falcón-Barroso J., Davies R. L., Bacon R., Bureau M., Cappellari M., de Zeeuw P. T., Emsellem E., Fathi K., Krajnović D., Kuntschner H., McDermid R. M., Peletier R. F., 2006, MNRAS , 366, 1151

Sembach K. R., Tonry J. L., 1996, AJ , 112, 797

Somerville R. S., Primack J. R., 1999, MNRAS , 310, 1087

Spitzer L. J., Baade W., 1951, ApJ , 113, 413

Tonry J. L., Dressler A., Blakeslee J. P., Ajhar E. A., Fletcher A. B., Luppino G. A., Metzger M. R., Moore C. B., 2001, ApJ , 546, 681

Trujillo I., Erwin P., Asensio Ramos A., Graham A. W., 2004, AJ , 127, 1917

Tully R. B., 1988, Nearby galaxies catalog. Cambridge and New York, Cambridge University Press, 1988, 221 p.

van den Bergh S., 1990, ApJ , 348, 57

van den Bosch F. C., Abel T., Croft R. A. C., Hernquist L., White S. D. M., 2002, ApJ , 576, 21

van der Marel R. P., Franx M., 1993, ApJ , 407, 525

van Driel W., Arnaboldi M., Combes F., Sparke L. S., 2000, A&AS , 141, 385

Vitvitska M., Klypin A. A., Kravtsov A. V., Wechsler R. H., Primack J. R., Bullock J. S., 2002, ApJ , 581, 799

Wernli F., Emsellem E., Copin Y., 2002, A&A , 396, 73

White S. D. M., 1984, ApJ , 286, 38

APPENDIX A: THE ANGULAR MOMENTUM OF GALAXIES AND λ_R

The criterion we wish to define should clearly separate the slow and fast rotators. The first guess is to take something equivalent to the total angular momentum, which should be expressed as something like $\langle X \cdot V \rangle$ where X is the distance to the spin axis. To avoid having to determine that axis, we chose $\langle R \cdot |V| \rangle$, where R is the distance to the centre. The absolute value of V is used as we are interested in the presence of local streaming motion (e.g. see NGC 4550). This is then naturally normalised by $\langle X \cdot \sqrt{\mu_2} \rangle$ where μ_2 is the second order moment $\mu_2 = V^2 + \sigma^2$.

However, another route would be to get closer to some physical quantity such as the angular momentum per unit mass. This can be represented via the spin parameter (e.g. Peebles 1969) defined as:

$$\lambda = \frac{J\sqrt{|E|}}{GM^{2.5}} \tag{A1}$$

where J, E, and M are the total angular momentum, energy and mass, and G is the Newton's constant. The derivation of λ in principle requires a robust distance for each galaxy. Since we wish to stay close to our SAURON measurements we need to define something which can be readily evaluated. This is possible by first rewriting λ as:

$$\lambda = \frac{J/M\sqrt{|E|/M}}{GM} \tag{A2}$$

For two-dimensional integral-field data, we can approximate the spin parameter by using the scalar virial relations and sky averaging over the field-of-view, weighted with the surface brightness. The scalar virial relations are $2E = -2K = W$, with the total kinetic and potential energy related to the mean-square speed of the system's stars $V_{\rm RMS}$ respectively as $2K/M = V^2_{\rm RMS}$ and $W/M = -GM/r_g$. Here, r_g is the gravitational radius, which can be related to the half-mass radius r_h given the mass model of the stellar system. For e.g. a spherical symmetric Jaffe (1983) model, we have $r_g = 2\,r_h$.

When relating r_g (or r_h) to the observed effective radius R_e, we have to take into account projection as function of the viewing angle of the stellar system which in in general is not spherical. Furthermore, while r_g (and r_h) are related to the mass distribution, R_e depends on the light distribution. Therefore, given $r_g = \kappa_R\,R_e$ the conversion factor κ_R is a function of the mass model, viewing direction and mass-to-light ratio. In a similar way a conversion factor is needed in the approximation of the total angular momentum by the observed radius time velocity: $J/M = \kappa_J\,R|V|$ (see Franx 1988). Furthermore, while $V^2_{\rm RMS}$ is the *total* mean-square speed, we only observe the second velocity moment projected along the line-of-sight, $V^2 + \sigma^2$. The latter should thus be multiplied with a factor $\kappa_K > 1$ (in the case of an isothermal sphere, $\kappa_K = 3$).

We thus find the following expressions:

$$J/M = \kappa_J\,\langle R|V|\rangle \tag{A3}$$

$$2E/M = -\kappa_K\,\langle (V^2+\sigma^2)\rangle \tag{A4}$$

$$GM = -r_g(W/M) = \kappa_R\kappa_K\langle R(V^2+\sigma^2)\rangle \tag{A5}$$

resulting in an approximate spin parameter

$$\lambda \sim \frac{\kappa_J}{\kappa_R\sqrt{2\kappa_K}}\,\lambda_f, \quad \text{with} \quad \lambda_f \equiv \frac{\langle RV\rangle\cdot\sqrt{\langle V^2+\sigma^2\rangle}}{\langle R\,(V^2+\sigma^2)\rangle}. \tag{A6}$$

which we then approximate by writing

$$\lambda_f \sim \lambda_R \equiv \frac{\langle RV\rangle}{\langle R\sqrt{V^2+\sigma^2}\rangle}$$

When deriving both the values of λ_f and λ_R for the 48 E and S0 SAURON galaxies, we indeed find a tight relation which can be written as:

$$\lambda_R \sim (0.95 \pm 0.04) \times \lambda_f \tag{A7}$$

This relation is in fact also valid for the two-integral models as derived in Appendix B, so that λ_R and λ_f are equal to within 10%.

For typical values of the conversion factors, $\kappa_J = 2$, $\kappa_K = 2$ and $\kappa_R = 3$, and we therefore find that $\lambda \sim \lambda_R/3$.

A simple approximation for the relation between λ_R and V/σ can then be obtained by simply ignoring the spatial averages from the definition of both parameters. In that case, we easily get:

$$\lambda_R = \frac{\langle RV\rangle}{\langle R\sqrt{V^2+\sigma^2}\rangle} \approx \frac{(V/\sigma)}{\sqrt{1+(V/\sigma)^2}} \tag{A8}$$

If we use the notation $\mathcal{F}(x) = x/\sqrt{1+x^2}$ we can write $\lambda_R \approx \mathcal{F}(V/\sigma)$. An alternative to λ_R is the unbounded $\lambda'_R = \frac{\langle RV\rangle}{\langle R\sigma\rangle} \approx (V/\sigma)$. In the context of early-type galaxies we favour λ_R which includes a mass-like normalisation by the second order moment $V^2+\sigma^2$. For isotropic (two-integral) models, this implies $\lambda_R \sim \sqrt{\epsilon}$.

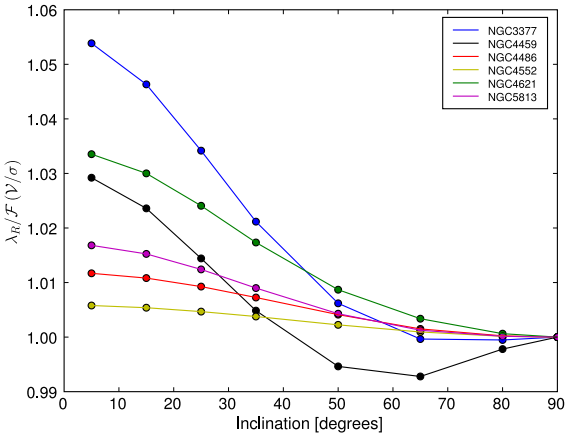

Figure B1. Ratio λ_R over $\mathcal{F}\,(V/\sigma)$, where $\mathcal{F}(x) = x/\left(1+x^2\right)$, derived from Jeans dynamical models of 6 galaxies of the SAURON E/S0 sample. This ratio is normalised for each galaxy to the value obtained for an edge-on view, and the result is shown with respect to the assumed viewing angle of the model.

APPENDIX B: TWO-INTEGRAL MODELS

In order to examine the behaviour of λ_R in more detail, we constructed two-integral dynamical Jeans models for 6 SAURON galaxies using the MGE formalism, namely NGC 524, 3377, 4459, 4486, 4552, 4621, and 5813. Details on the assumptions and resulting mass models for these galaxies can be found in Paper IV. For each galaxy, we assumed 8 different viewing angles (5, 15, 25, 35, 50, 65, 80, and 90°, the latter corresponding to an edge-on view), and derived the first two line-of-sight velocity moments up to 1 Re.

These models were then used to obtain measurement of λ_R and V/σ, to determine whether these two quantities behave similarly with respect to basic parameters such as the inclination or anisotropy parameter. As shown in Fig. B1, the variation of λ_R with inclination follows that of V/σ within 10%. This result does not depend on the anisotropy, as long as the internal dynamics of the model is fixed before changing the viewing angle. It is however clear that a radial variation in the anisotropy profile can significantly change this ratio, as λ_R includes an additional explicit dependence on radius. Even assuming isotropy for all 6 MGE Jeans models, we observe a spread of about 40% in the values of the ratio $\lambda_R/\mathcal{F}\,(V/\sigma)$ (see Appendix A), showing evidence that non-homology is an important driver of changes in λ_R at constant V/σ.

Another important issue when deriving λ_R and V/σ comes from the presence of noise in the measurements. When V is sufficiently large, the random errors in the kinematic measurements will affect both λ_R and V/σ randomly. As V becomes small in absolute value, $\langle V^2\rangle$ and $\langle R\cdot V\rangle$ become increasingly biased (being artificially increased), which affects estimates of λ_R and V/σ. In Fig. B2, we show the effect of a random error of 10 km s^{-1} in both V and σ (typical in the outer part of SAURON kinematic maps; see Paper III) on both λ_R and V/σ, in terms of λ_R. Δ is the difference between the measured value (with noise) and the expected one (noiseless) and is plotted with respect to the true λ_R value. The effect is in general relatively small, of the order of 7% on λ_R and almost 15% on V/σ, for $\lambda_R \sim 0.1$. When V is close to zero everywhere, as is the case for the three SAURON galaxies with the lowest λ_R values, the presence of noise yields an overestimate of about

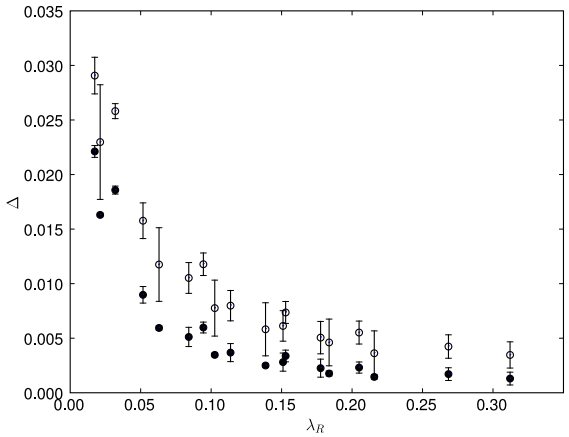

Figure B2. Effect of noise in the kinematics on the estimate of λ_R (filled symbols) and V/σ (empty symbols). Δ, the difference between the measured value (with noise) and the expected one (noiseless), is plotted against λ_R. The input noise has been set to 10 km s^{-1} for both V and σ.

0.02 in λ_R (depending on the velocity dispersion values), an effect consistent with the observed values for these galaxies (see Fig. 3). As expected, Fig. B2 also shows that λ_R is in general about a factor of two less sensitive to errors in the kinematic measurements than V/σ.